

Global Biogeochemical Cycles®

RESEARCH ARTICLE

10.1029/2023GB007841

Key Points:

- Nutrient enrichment in the surface seawater driven by upwelling and atmospheric deposition promoted the biological production of isoprene
- Photochemical production was confirmed as an abiotic source of marine isoprene
- Approximately 10%~63% of net isoprene produced in the mixed layer was transferred to the atmosphere

Supporting Information:

Supporting Information may be found in the online version of this article.

Correspondence to:

H.-H. Zhang and Z.-H. Chen,
honghaizhang@ouc.edu.cn;
chenzhaohui@ouc.edu.cn





Citation:

Wang, J., Zhang, H.-H., Booge, D., Zhang, Y.-Q., Li, X.-J., Wu, Y.-C., et al. (2023). Isoprene production and its driving factors in the Northwest Pacific Ocean. *Global Biogeochemical Cycles*, 37, e2023GB007841. <https://doi.org/10.1029/2023GB007841>

Received 10 MAY 2023

Accepted 18 NOV 2023

Isoprene Production and Its Driving Factors in the Northwest Pacific Ocean

Jian Wang¹, Hong-Hai Zhang¹ , Dennis Booge² , Yue-Qi Zhang³ , Xiao-Jun Li¹, Ying-Cui Wu¹, Jia-Wei Zhang⁴, and Zhao-Hui Chen³ 

¹Frontiers Science Center for Deep Ocean Multispheres and Earth System, Key Laboratory of Marine Chemistry Theory and Technology, Ministry of Education, Ocean University of China, Qingdao, China, ²GEOMAR Helmholtz Center for Ocean Research Kiel, Kiel, Germany, ³Key Laboratory of Physical Oceanography, Ministry of Education, Ocean University of China, Qingdao, China, ⁴Eco-Environmental Monitoring and Research Center, Pearl River Valley and South China Sea Ecology and Environment Administration, Ministry of Ecology and Environment, Guangzhou, China

Abstract Marine isoprene plays a crucial role in the formation of secondary organic aerosol within the remote marine boundary layer. Due to scarce field measurements of oceanic isoprene and limited laboratory-based studies of isoprene production, assessing the importance of marine isoprene on atmospheric chemistry and climate is challenging. Calculating in-field isoprene production rates is a crucial step to predict marine isoprene concentrations and the subsequent emissions to the atmosphere. The distribution, sources, and dominant environmental factors of isoprene were determined in the Northwest Pacific Ocean in 2019. The nutrient enrichment in the Kuroshio Oyashio Extension (KOE) surface seawater, driven by the upwelling and atmospheric deposition, promoted the growth of phytoplankton and elevated the isoprene concentration. This was confirmed by observed responses of isoprene to nutrients and aerosol dust additions in a ship-based incubation experiment, where the isoprene concentrations increased by 70% ($t = 4.417$, $p < 0.001$) and 35% ($t = 2.387$, $p < 0.05$), respectively. Biogenic isoprene production rates in the deck incubation experiments were positively related to chlorophyll *a*, temperature, and solar radiation, with an average production of 7.33 ± 4.27 pmol L⁻¹ day⁻¹. Photochemical degradation of dissolved organic matter was likely an abiotic source of isoprene, contributing to approximately 14% of the total production. Driven by high isoprene production and extreme physical disturbance, the KOE showed very high emissions of isoprene of 46.0 ± 13.0 nmol m⁻² day⁻¹, which led to a significant influence on the oxidative capacity of the local atmosphere.

1. Introduction

Isoprene (C₅H₈), one of the most abundant biogenic volatile organic compounds, has significant influence on atmospheric chemistry and global climate regulation. Atmospheric isoprene reacts with hydroxyl radicals and nitrogen oxides, which alter the oxidative capacity of the atmosphere (Liakakou et al., 2007; Paulot et al., 2012; Wennberg et al., 2018) and forms ozone (Houweling et al., 1998; Poisson et al., 2000). In addition, isoprene oxidation products are vital precursors of many secondary organic aerosols (Fry et al., 2018; Hu et al., 2013) that act as cloud condensation nuclei, which impact both air quality and global radiation budgets (Carslaw et al., 2010).

Marine phytoplankton have been shown to be important sources of atmospheric isoprene, as has been demonstrated by laboratory experiments that have estimated the biological production rates of isoprene (0.72~32.1 pmol C₅H₈ μg Chl-*a*⁻¹ day⁻¹) (Bonsang et al., 2010; Exton et al., 2013; Gantt et al., 2009; McKay et al., 1996; Meskhidze et al., 2015; Shaw et al., 2003). The isoprene production rates in seawater (0.40~60.5 pmol C₅H₈ μg Chl-*a*⁻¹ day⁻¹) have been indirectly estimated on the basis of sea-to-air fluxes and consumption rates, assuming that the production is balanced by all consumption/loss processes (Booge et al., 2018; Ooki et al., 2015; Simó et al., 2022). However, in situ production rates of isoprene in natural seawater are rarely reported, which exacerbates the uncertainty in models established to quantify global marine isoprene emissions. Additionally, a photo-sensitized reaction in the sea-surface microlayer was shown to produce significant amounts of isoprene (Ciuraru et al., 2015), which makes it a possible abiotic source of isoprene in marine environments. Given the potential variety of isoprene sources, it is necessary to directly determine isoprene production rates and explore potential additional contributors to marine isoprene production.

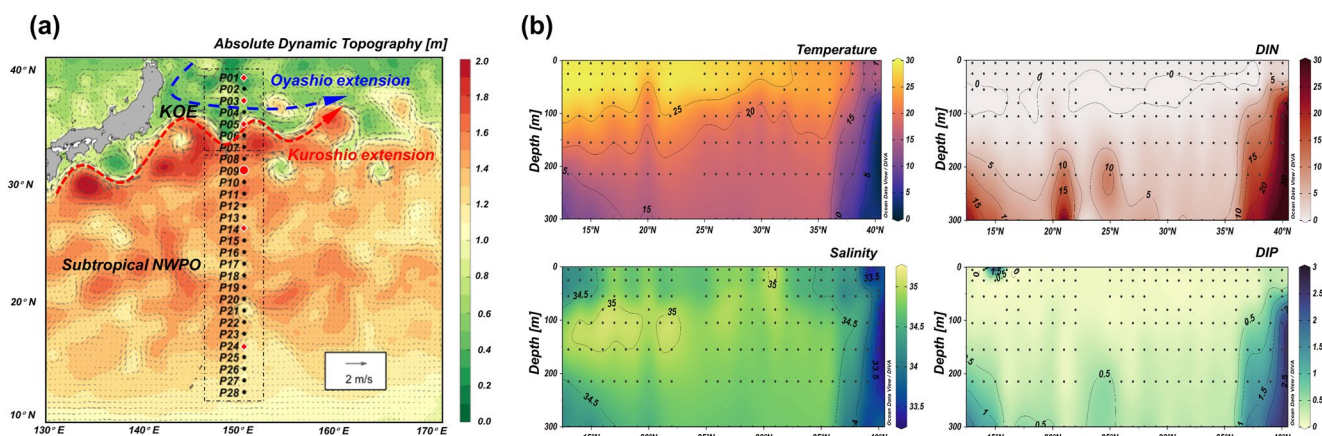


Figure 1. (a) Surface geostrophic currents in the Northwest Pacific Ocean during the cruise. Vectors reflect flow rates of surface currents. Absolute dynamic topography data were downloaded from <https://resources.marine.copernicus.eu>. Red diamonds (◆) and dots (●) indicate the stations for rate measurements and incubation experiments, respectively. (b) Section plots of temperature (°C), salinity, dissolved inorganic phosphorus (DIP) ($\mu\text{mol L}^{-1}$), and dissolved inorganic nitrogen (DIN) ($\mu\text{mol L}^{-1}$).

The Northwest Pacific Ocean (NWPO) is a unique region characterized by an intricate system of currents and perennial hurricanes. As the main current that connects prominent oceanic gyres in the NWPO (Lu et al., 1998), the Kuroshio Oyashio Extension (KOE) is disturbed by persistent eddies that exert significant impacts on heat transport, surface winds, and rainfall (Frenger et al., 2013; Ma et al., 2016), while also supplementing the euphotic layer with nutrients (Siegel et al., 1999). In addition, dust deposition from East Asia also supplies nutrients to the NWPO at different times of the year (Martino et al., 2014; Seok et al., 2021). These marine and atmospheric activities play vital roles in regulating local marine ecosystems, which subsequently influence the production and emission of biological isoprene. Here, we investigated the spatial variation in isoprene and environmental parameters in the NWPO as well as the response of marine isoprene production to environmental changes via onboard incubation experiments. Simultaneously, we determined the isoprene production rates from biogenic and photochemical processes and estimated the column-integrated production of isoprene in the mixed layer.

2. Methods

2.1. Voyage and Sampling

Comprehensive isoprene research was conducted in the NWPO on board the R/V “*Dongfanghong 3*” from 2 October to 1 November 2019. The study area and sampling locations are shown in Figure 1a. Separate surface seawater samples for isoprene, nutrients, chlorophyll-*a* (Chl-*a*), and phytoplankton were collected from 26 surface and vertical stations using Niskin bottles (12L) on a sampling rosette. The temperature and salinity of seawater were measured using a conductivity-temperature-depth (CTD) instrument cluster (Seabird911) at the time of sampling. Data of net solar radiation and wind speed were obtained from the ship's meteorological station.

2.2. Analysis of Isoprene in Seawater

Isoprene in seawater was measured immediately on board using a purge and trap system coupled with a gas chromatographer equipped with a flame ionization detector (GC-FID, 7890B, Agilent). The purge and trap system was improved on the basis of a previous device designed in the laboratory described by Li et al. (2019). Briefly, seawater was collected using a customized glass sampler (500 mL) and was connected to the inlet of the system. Then the seawater was transferred into the extraction cell under pressure from pure N₂ and was purged with a flow of pure N₂ bubbles (250 mL min⁻¹). The moisture of the carrier gas condensed as it passed through a thin glass tube held in a cold chamber (4~6°C). Carbon dioxide in the carrier gas was absorbed using a glass tube filled with Ascarite II (Merck). The isoprene was then concentrated in a passivated stainless steel tube immersed in liquid nitrogen for 26 min. Then, the steel tube was heated in boiling water and the six-way valve was opened to the inlet of the analyzer. The concentrated gases were transferred into the Rt-Alumina BOND/KCl capillary column (50 m × 0.32 mm × 5 μm, Agilent) for separation and were determined by the FID. The parameters of

the inlet, oven, and detector are shown in Table S1 in Supporting Information S1. The gas standard (Linde Gases, Germany) was diluted using pure N₂ to 10 parts per billion (ppb) for identification and quantification. Instrumental blank was used to guarantee data reliability. The precision and detection limits were 3% and 0.5 pmol L⁻¹, using a sample volume of 500 mL.

2.3. Analysis of Chl-*a*, Nutrients, Absorption Coefficients, and Phytoplankton

For Chl-*a* analysis, 1 L seawater was filtered through a GF/F membrane (0.70 μm pore size, Whatman). The filter was folded and placed into a 15 mL centrifuge tube that was wrapped with tinfoil. 10 mL acetone solution (90%) was added to the centrifuge tube for Chl-*a* extraction. After 24 hr, the tubes were centrifuged, and the fluorescence intensity of the supernatant was measured using a fluorescence spectrophotometer (F-4700, Hitachi). For nutrient analysis, 50 mL seawater was collected in a polyethylene bottle and the concentrations of NO₃⁻, NO₂⁻, and PO₄³⁻ were determined using an auto-analyzer (AA3, Seal). For phytoplankton analysis, 1 L seawater was collected and fixed with 10 mL Lugol's solution. Phytoplankton samples were stored in the dark and concentrated to 10~15 mL in the laboratory using the sedimentation method. The absorption coefficient of filtered seawater (0.7 μm pore size, GF/F membrane) was measured to calculate the light attenuation within the water column. The absorption spectra were determined using a UV-Vis spectrophotometer (UV-2550, Shimadzu) across the wavelength range from 200 to 800 nm. The filtered seawater samples were calibrated against a 10 cm quartz cuvette containing Milli-Q water as the reference solution. Phytoplankton species were identified and cell numbers were counted using a phytoplankton enumeration chamber under a microscope (Olympus BX51, Olympus).

2.4. Determination of Isoprene Production Rates

2.4.1. Photochemical Production Rate

Isoprene production rate experiments were conducted onboard the NWPO using seawater collected from the Niskin bottles from 5 m depth. Natural seawater was filtered through a polycarbonate filter (0.22 μm, Millipore). Quartz bottles (550 mL) were filled with filtered seawater of known isoprene concentration and exposed to solar radiation or kept in the dark for incubation in triplicate. All bottles were completely filled to prevent isoprene loss to the head space. To maintain in situ temperatures in the exposed bottles, bottles were placed on the deck in a 0.5 m depth water bath that was continuously flushed with surface seawater. The water bath was covered by a neutral density screen to attenuate the light intensity by around 40% to avoid an overestimation of isoprene production in the water column. Guo et al. (2012) and Zhang et al. (2019) have proved that ~40% light attenuation is suitable for collecting seawater at 5 m depth to conduct deck incubation experiments. Light experiments were conducted for 6 hr during a period of intense light from 9:00 to 15:00 local time. The diurnal variations of light intensity during the experiments are shown in Figure S1 in Supporting Information S1. The filtered seawater was expected to contain viruses, few microbes, and no phytoplankton (Ratte et al., 1993). Since the role of viruses in isoprene production or consumption is still unclear, and there are no relevant studies, we ignored the influence of viruses on the production processes of isoprene in seawater. The effects of few microbes and chemical oxidation on isoprene were eliminated according to the control groups (discussed in Section 3.3). However, there might be photo-degradation of isoprene during the light cultivation process, and this aspect has not been accurately assessed or excluded in this study. Therefore, the ultimate photochemical production of isoprene should be considered as a net production encompassing a potential photochemical degradation component. Additionally, the proportion of solar radiation during 6-hr incubation to the total radiation in a day was calculated using the net solar radiation data from the ship's meteorological station. We divided the increase in isoprene concentration using this proportion to determine the daily photochemical production rate of isoprene in filtered seawater (P_{photo} , pmol L⁻¹ day⁻¹), on the assumption that photochemistry is proportional to light intensity.

2.4.2. Biological Production Rate

Similar to the determination of the photochemical isoprene production rate, quartz bottles were filled completely with natural seawater (unfiltered) with a known isoprene concentration and exposed to solar radiation in a water bath. In this scenario, ignoring the negligible effect of viruses, the processes affecting isoprene concentrations in the bottles should be limited to phytoplankton production, photochemical production, microbial consumption, and chemical oxidation. Therefore, any increase in isoprene per unit time ($P_{\text{determine}}$, pmol L⁻¹ day⁻¹) can be considered as the net production rate of natural seawater in the quartz bottles, as described in Equation 1:

$$P_{\text{determine}} = P_{\text{bio}} + P_{\text{photo}} - L_{\text{loss}} \quad (1)$$

Table 1
*Mixed Layer Depth, Chl-*a*, Production Rates, and Sea-To-Air Fluxes of Isoprene at Incubation Stations*

Station	Depth of mixed layer m	Chl- <i>a</i> $\mu\text{g L}^{-1}$	Surface water			Mixed layer		Sea-to-air flux $\text{nmol m}^{-2} \text{day}^{-1}$
			P_{bio} $\text{pmol L}^{-1} \text{day}^{-1}$	P_{photo} $\text{pmol L}^{-1} \text{day}^{-1}$	P_{bio}^* $\text{pmol } \mu\text{g Chl-}a^{-1} \text{day}^{-1}$	$P_{\text{bio-total}}$ $\text{nmol m}^{-2} \text{day}^{-1}$	$P_{\text{photo-total}}$ $\text{nmol m}^{-2} \text{day}^{-1}$	
P01	41	0.47	11.3	1.25	24.2	156	13.5	40.9
P03	18	0.52	6.89	1.44	13.4	111	13.2	47.0
P05	72	0.62	13.0	1.14	21.1	611	13.0	59.2
P14	49	0.11	3.25	1.48	28.4	128	16.6	21.1
P24	34	0.06	2.17	1.18	38.5	28.5	12.7	26.1

Note. P_{bio} and P_{photo} are biogenic and photochemical production rates of isoprene in surface seawater. P_{bio}^* is the biogenic production rate per unit of Chl-*a*. $P_{\text{bio-total}}$ and $P_{\text{photo-total}}$ are column-integrated production rates driven by phytoplankton and photochemistry, respectively.

Equation 1 could be transformed into “ $P_{\text{bio}} = P_{\text{determine}} - P_{\text{photo}} + L_{\text{loss}}$ ” to calculate the biological production rate of isoprene from phytoplankton (P_{bio} , $\text{pmol L}^{-1} \text{day}^{-1}$). P_{photo} is the photochemical production rate of isoprene by degradation of dissolved organic matter (DOM) and L_{loss} is the isoprene loss rate, which includes chemical oxidation and microbial consumption. Although we showed that the chemical oxidation of isoprene can be ignored over short time periods, as shown in the filtered seawater dark incubation experiment, it is hard to isolate microbes from phytoplankton in seawater to quantify their consumption or production rates separately. Therefore, the P_{bio} value can be seen as the minimum biological production rate of isoprene.

2.5. Column-Integrated Isoprene Production Rate in the Mixed Layer

Isoprene is thought to be mainly produced within the mixed layer of the ocean. Characterizing the production patterns of isoprene within the mixed layer helps evaluate the overall budget of isoprene in the marine environment. Through measurements or simulations accounting for variations in light intensity, temperature, and Chl-*a* within the mixed layer, we calculated the isoprene production rates at different depths by establishing the relationship between isoprene production and environmental parameters.

2.5.1. Photochemical Production

The mixed layer depth (MLD, given in Table 1) is defined by a set temperature decrease ($\Delta T = 0.2^\circ\text{C}$) from the value at 10 m depth (de Boyer Montegut et al., 2004). DOM is assumed to be homogeneously distributed in the mixed layer, and the photochemical production of isoprene results from the transformation of DOM driven by solar radiation. When the DOM concentration is constant, the photochemical production of isoprene is proportional to the light intensity. Furthermore, a study on diurnal variability reported that experimentally determined production rates of alkene in quartz glass bottles were very similar to those from field measurements (Ratte et al., 1993). Thus, the isoprene production rate in quartz glass bottles can effectively approximate the isoprene production rates of the surface seawater.

The column-integrated isoprene production rates per unit area of sea surface can be calculated using the following equation:

$$P_z = P_0 \frac{I_z}{I_0} \quad (2)$$

where I_0 and I_z are the light intensities at the sea surface and depth z , respectively; P_0 is the photochemical production rate in the surface seawater; and P_z is the photochemical isoprene production rate at depth z .

According to the Beer-Lambert law, the relationship between light intensity at depth z and that at the sea surface can be written as Equation 3:

$$I_z = I_0 \times e^{-k_x z} \quad (3)$$

Due to huge discrepancies in the attenuation coefficients of light in different wavelength bands within seawater, we separated the calculated attenuation of ultraviolet radiation (UV) and photosynthetically active radiation

(PAR) to determine the light intensity at a given depth z , like Equation 4. Light with wavelength exceeding 700 nm was disregarded due to its lower energy which limits its potential to induce photochemical reactions. In Equation 5, $\alpha_w(\text{UV})$ and $\alpha_{\text{CDOM}}(\text{UV})$ are the absorption coefficients of pure water and chromophoric DOM under the UV light, respectively. We measured the absorption coefficients of filtered seawater samples for light wavelengths ranging from 200 to 800 nm, selecting a 350 nm absorption coefficient to compute UV attenuation and 550 nm for PAR attenuation. Additionally, the PAR attenuation is influenced by phytoplankton, which is presumed to be proportional to the Chl- a concentration ($[\text{CHL}]$, mg L^{-1}) (Kloster et al., 2006), as shown in Equation 6. k_{UV} was in the range of 0.0860–0.0900 m^{-1} and k_{PAR} of 0.0157–0.0615 m^{-1} , with the specific data listed in the Table S3 in Supporting Information S1. The surface UV ($I_{0(\text{UV})}$) and PAR radiation ($I_{0(\text{PAR})}$) were calculated based on the typical proportions of UV and PAR within the solar radiation, which are conventionally estimated at 8% and 40%, respectively (Stamnes, 2015).

$$I_z = I_{0(\text{UV})} \times e^{-k_{\text{UV}}z} + I_{0(\text{PAR})} \times e^{-k_{\text{PAR}}z} \quad (4)$$

$$k_{\text{UV}} = \alpha_w(\text{UV}) + \alpha_{\text{CDOM}}(\text{UV}) \quad (5)$$

$$k_{\text{PAR}} = \alpha_w(\text{PAR}) + \alpha_{\text{CDOM}}(\text{PAR}) + 0.03 \times [\text{CHL}] \quad (6)$$

Finally, the column-integrated photochemical production rate in the mixed layer ($P_{\text{photo-total}}$, $\text{nmol m}^{-2} \text{day}^{-1}$) is calculated using Equation 7:

$$P_{\text{photo-total}} = \int_0^D P_0 \times \frac{I_{0(\text{UV})} \times e^{-k_{\text{UV}}z} + I_{0(\text{PAR})} \times e^{-k_{\text{PAR}}z}}{I_{0(\text{UV})} + I_{0(\text{PAR})}} \times dz \quad (7)$$

2.5.2. Biological Production

As shown in Equation 8, according to the experiments of biological isoprene production rate, we fit the function of biological production rate normalized by Chl- a (P_{bio}^* , $\text{pmol } \mu\text{g Chl-}a^{-1} \text{day}^{-1}$) depending on seawater temperature (T , $^{\circ}\text{C}$) and light intensity (I , W m^{-2}). Figure 4d shows the fitting result between predicted and measured values.

$$P_{\text{bio}}^* = 0.719 \times T + 0.038 \times I - 2.97 \quad (8)$$

Thus, the calculation of the column-integrated biological production rate of isoprene ($P_{\text{bio-total}}$, $\text{nmol m}^{-2} \text{day}^{-1}$) can be determined using Equation 9. I_z is the light intensity at depth z and is still calculated using Equation 3. T_z and $[\text{CHL}]_z$ are the seawater temperature and Chl- a at depth z , respectively. Temperature data is used from the CTD temperature profile at high resolution. Chl- a data is used from regular CTD bottle sampling depth as shown in Figure 6.

$$P_{\text{bio-total}} = \int_0^D (0.719 \times T_z + 0.038 \times I_z - 2.97) \times [\text{CHL}]_z \times dz \quad (9)$$

2.6. Calculation of Sea-To-Air Flux

The sea-to-air flux of isoprene (F , $\text{nmol m}^{-2} \text{day}^{-1}$) was calculated using Equation 10:

$$F = k \times (C_w - C_a \times H) \quad (10)$$

where k (m s^{-1}) is the gas transfer velocity; H is Henry's law constant; C_w (pmol L^{-1}) is the isoprene concentration in seawater; and C_a (ppb) is the mixing ratio of isoprene in the atmosphere, in this case referring to the average mixing ratio of atmospheric isoprene (0.225 ppb) in the Western Pacific Ocean (Li et al., 2019).

$$k = 0.31 \times u^2 \times \left(\frac{\text{Sc}}{660} \right)^{-0.5} \quad (11)$$

where u (m s^{-1}) is the wind velocity at 10 m; Sc is the Schmidt number, defined as $\text{Sc} = \mu/D$; μ is the kinematic viscosity of seawater (Wanninkhof, 1992); and D is the diffusion coefficient of isoprene related to temperature (Wilke & Chang, 1955).

$$\mu = 1.052 + 1.300 \times 10^{-3} \times t + 5.000 \times 10^{-6} \times t^2 + 5.000 \times 10^{-7} \times t^3 \quad (12)$$

$$D = \frac{7.4 \times 10^{-8} (q \times M_b)^{0.5} \times T}{n_b \times V_a^{0.6}} \quad (13)$$

where t (°C) is the temperature of seawater in Celsius; q is the association factor of water; M_b (g mol⁻¹) is the molar weight of water; T (K) is the temperature of seawater in Kelvin; n_b is the dynamic viscosity of seawater; and V_a is the molar volume at the boiling point.

2.7. Incubation Experiment

A 22-day incubation experiment was conducted during the cruise to explore the impacts of environmental factors on marine isoprene concentrations. Seawater was collected from a depth of 5 m at station P09 (150°E, 31°N) in the Low Nutrients Low Chlorophyll region. The concentrations of dissolved inorganic nitrogen (DIN), dissolved inorganic phosphorus (DIP), and Chl-*a* in the seawater were 0.04 μmol L⁻¹, 0.07 μmol L⁻¹, and 0.115 μg L⁻¹, respectively. After being filtered through a 200 μm nylon mesh, seawater was transferred into 20 L polycarbonate bottles. To keep temperatures at in situ levels during the experiment, bottles were placed in a 0.5 m depth water bath that was continuously flushed with surface seawater. The water bath was covered by a neutral density screen similar to the incubation experiments in “Section 2.4.” Three groups of bottles were set up (in triplicate). M1 was the control group, M2 was enriched with nutrients to replicate the surface seawater in the KOE (nitrate: 4.00 μmol L⁻¹; phosphate: 0.25 μmol L⁻¹), and M3 had aerosol dust added. The aerosol dust had been collected in advance from the East China Sea in the summer of 2018 using a high-volume total suspended particulate sampler (Model KB-1000, Jinshida Electronic Technology) with cellulose 41 filters (20 × 25 cm², Whatman) serving as the substrates, at an airflow rate of about 1.0 m³ min⁻¹ for 24 hr. The dust sample was dissolved in 100 mL deionized water and sonicated for 1 hr at 0°C. Then, the suspension was added to incubation bottles. The initial concentration of aerosol dust in the M3 bottles was set to 2.0 mg L⁻¹, representing a case of strong aerosol deposition (Zhang et al., 2019). Samples were collected from bottles for measurements of isoprene, Chl-*a*, nutrients, and phytoplankton abundance every 2 or 3 days.

3. Results

3.1. Isoprene and Environmental Parameters in the NWPO

Based on the geostrophic surface currents (Figure 1a) and the temperature and salinity characteristics (Figure 1b), we partitioned the research transect into two distinct regions. The area with greater surface current flow rates and larger variability in surface temperature and salinity was identified as the KOE. The hydrodynamic features of this region were predominantly driven by the activities of Oyashio and Kuroshio extension. The southern area with a gentle current rate and homogenous temperature and salinity distributions was identified as the subtropical NWPO. As demonstrated in the thermohaline vertical profiles (Figure 1b), we observed an upwelling action at 35–40°N, characterized by temperatures below 10°C and salinity below 33.5 in the KOE. This upwelling featured concentrations of DIN and DIP at 1.48 ± 0.60 and 19.1 ± 7.12 μmol L⁻¹, respectively, with an N:P ratio of 13:1 approximating the Redfield ratio.

The DIN and DIP concentrations (mean ± SD) of surface seawater (5 m depth) in the KOE were 0.81 ± 1.14 and 0.18 ± 0.11 μmol L⁻¹, respectively, while those in the subtropical NWPO were 0.06 ± 0.08 μmol L⁻¹ and 0.07 ± 0.01 μmol L⁻¹. The Chl-*a* concentration in the surface seawater (5 m depth) in the KOE (0.46 ± 0.14 μg L⁻¹) was significantly higher than that in the subtropical NWPO (0.063 ± 0.029 μg L⁻¹) ($t = 11.23$, $p < 0.001$). Similarly, the cell density of phytoplankton in the surface seawater in the KOE [(3.6 ± 3.1) × 10⁴ cell L⁻¹] was approximately 10 times that in the subtropical NWPO [(3.3 ± 2.1) × 10³ cell L⁻¹]. The surface isoprene concentration in the KOE (14.3 ± 2.41 pmol L⁻¹) was higher than that in the subtropical NWPO (11.9 ± 2.40 pmol L⁻¹) ($t = 2.141$, $p = 0.043$), which corresponded to the patterns in Chl-*a* and phytoplankton cell density (Figure 2).

3.2. Variations of Isoprene Concentration to Additions of Nutrients and Aerosol Dust

To discern the specific impacts of nutrients (from upwelling) and aerosol dust (from atmospheric deposition) on marine isoprene production, ship-based incubation experiments were conducted to monitor isoprene concentrations after the addition of nutrients and aerosol dust.

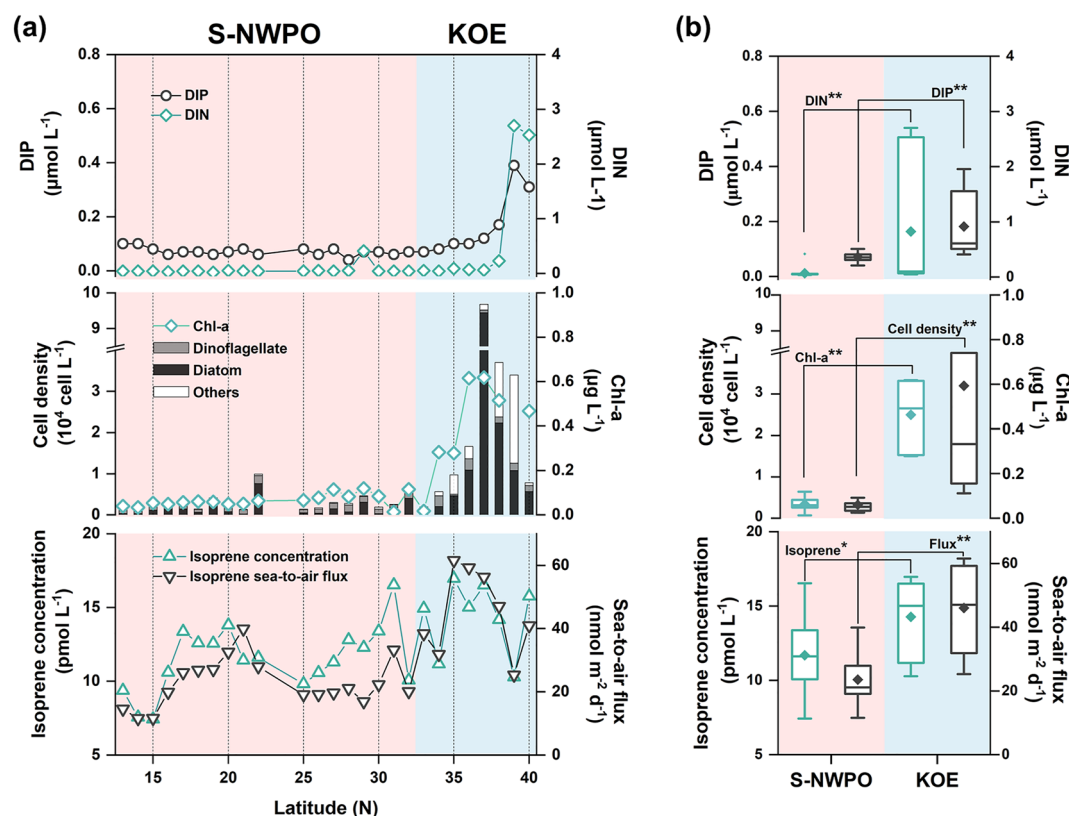


Figure 2. (a) Surface distribution (5 m depth) of dissolved inorganic phosphorus (DIP), dissolved inorganic nitrogen (DIN), cell density, Chl-*a*, isoprene, and sea-to-air flux of isoprene along 150°E (b) Box plots of DIP, DIN, Chl-*a*, cell density, isoprene, and sea-to-air flux of isoprene in surface seawater in the Kuroshio Oyashio Extension (KOE) ($n = 7$) and the subtropical Northwest Pacific Ocean (NWPO) ($n = 19$). The lines of the boxes represent the 25th (bottom), 50th (middle), and 75th (top) percentiles, respectively; the whisker caps represent the 5th and 95th percentiles; and the black solid diamonds represent the mean value. * and ** represent significant differences between groups at the $p < 0.05$ and $p < 0.01$ levels, respectively.

3.2.1. Control Group

Seawater, without additional treatment, was cultivated over the entire period of the incubation experiment and served as the control group (M1). During the first 10 days, the mean concentration of DIP was $0.03 \pm 0.02 \mu\text{mol L}^{-1}$, while the concentrations of DIN were almost below the detection limit. This restricted the growth of phytoplankton in this period, with the mean Chl-*a* concentration and cell density decreasing to $0.07 \pm 0.03 \mu\text{g L}^{-1}$ and $417 \pm 329\text{-cell L}^{-1}$. However, there was a slight increase in DIN and DIP (Figures 3i and 3m) after 10 days, which was also found in M2 treatment (Figures 3j and 3n). The decomposition of organic matter by bacteria induced a rise in nutrient levels, similar to the regeneration of nutrients in the upper ocean. These self-replenished nutrients enhanced the cell density of phytoplankton to $1,517 \pm 1,221\text{-cell L}^{-1}$ (mainly *Chaetoceros* sp.) in the stage after 10 days, but values were still significantly lower than that in M2 and M3. The isoprene concentration in M1 was the lowest, with an average of $11.3 \pm 4.45 \text{ pmol L}^{-1}$ during the entire incubation experiment.

3.2.2. Nutrient Addition

In the M2 treatment, nutrients were enriched to levels comparable to those in surface waters of the KOE. During the first 4 days, the averages of DIN and DIP were 4.11 ± 1.36 and $0.17 \pm 0.06 \mu\text{mol L}^{-1}$, but subsequently declined afterward (Figures 3j and 3n). After 10 days, the concentrations decreased to 0.41 ± 0.35 and $0.06 \pm 0.04 \mu\text{mol L}^{-1}$, respectively. The Chl-*a* concentrations increased exponentially at the beginning of the experiments (Figure 3f) and peaked at $1.65 \pm 0.44 \mu\text{g L}^{-1}$ on day 6. During this period, diatoms (mainly *Cylindrotheca closterium* and *Rhizosolenia delicatula*) were predominant and there was an extremely large diatom/dinoflagellate ratio of 924:1. The changing trend in isoprene was similar to that of Chl-*a* (Figure 3r), but

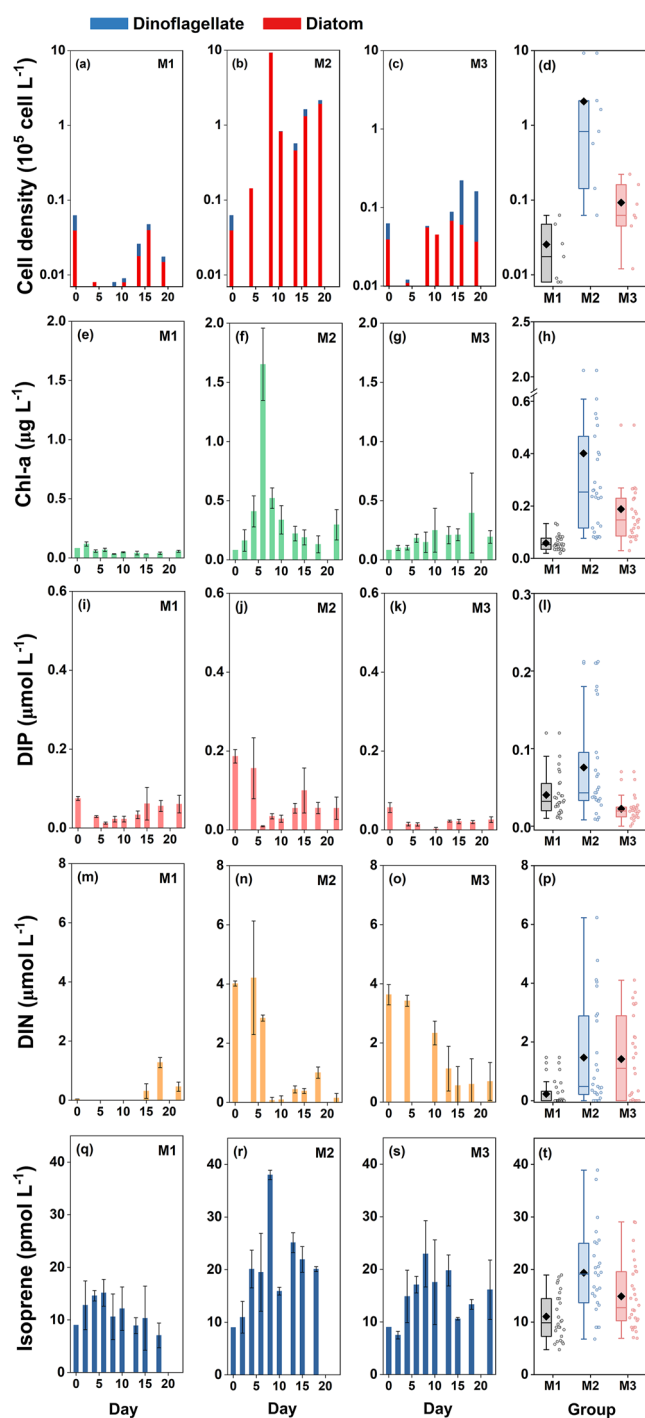


Figure 3. Temporal changes (first to third columns) and box charts (fourth column) of isoprene, Chl-*a*, cell density, dissolved inorganic nitrogen (DIN), and dissolved inorganic phosphorus (DIP) in different treatments. M1, control; M2, nutrient enrichment; M3, aerosol dust addition. Phytoplankton composition was determined only in one of the replicates. Error bars of columns are the standard deviation from triplicate measurements. The lines in the boxes represent the 25th (bottom), 50th (middle), and 75th (top) percentiles, respectively; the whisker caps represent the 5th and 95th percentiles; black solid diamonds represent the mean values; and circles to the right of the boxes represent the actual data.

concentrations ($38.0 \pm 0.89 \text{ pmol L}^{-1}$) peaked 2 days after Chl-*a*. After the nutrients had been depleted, Chl-*a* and isoprene decreased to low concentrations in the later incubation period. Although the cell density of diatoms decreased in the later stage of the experiment, they were still predominant (mainly *Chaetoceros pelagicus* and *Chaetoceros pseudocurvisetus*), accounting for around 86% of the total cell density. The mean concentrations of both Chl-*a* ($t = 3.946$, $p < 0.001$) and isoprene ($t = 4.417$, $p < 0.001$) were significantly higher in the nutrient treatments (M2) compared to the control treatments (M1).

3.2.3. Dust Aerosol Addition

Pre-treated aerosol sample extracts were added to treatment M3 to simulate a strong aerosol deposition in the upper ocean. The addition of dust aerosol appeared to introduce nutrients to the M3 treatment. The initial concentrations of DIN and DIP were 3.63 ± 0.34 and $0.06 \pm 0.01 \mu\text{mol L}^{-1}$, respectively, indicating DIN values similar to the M2 treatment but a notably phosphorus (P) limitation (Figures 3k and 3o). Chl-*a* concentrations increased slowly from the beginning to the end of the incubation period (Figure 3s), but no obvious phytoplankton bloom occurred due to the P limitation. The phytoplankton community composition in M3 was dominated by diatoms (mainly *C. closterium* and *Chaetoceros* sp.) until day 12, after which there was a significant increase in dinoflagellates (mainly *Karenia brevis* and *Karenia digitata*) (Figure 3c). Finally, dinoflagellates became dominant after day 14 and accounted for about 75% of the total cell density at the later stage of the incubation. The isoprene concentration peaked on day 8 ($24.6 \pm 4.12 \text{ pmol L}^{-1}$). After reaching its low point ($10.6 \pm 0.25 \text{ pmol L}^{-1}$) on day 15, isoprene increased again at the end of the incubation. The average isoprene concentration was about 35% higher in M3 than in the control treatment M1 ($t = 2.387$, $p < 0.05$).

3.3. Biological and Photochemical Production Rates of Isoprene

The production rates of marine isoprene in surface seawater were determined through 6-hr incubations (Table 1). The biological production rates of isoprene (P_{bio}) ranged from 2.17 to $13.0 \text{ pmol L}^{-1} \text{ day}^{-1}$ with a mean value of $7.33 \pm 4.27 \text{ pmol L}^{-1} \text{ day}^{-1}$. Biological production rates of isoprene in the KOE ($10.4 \pm 2.57 \text{ pmol L}^{-1} \text{ day}^{-1}$) were larger than those in the subtropical NWPO ($2.71 \pm 0.54 \text{ pmol L}^{-1} \text{ day}^{-1}$), which was consistent with the distribution of phytoplankton abundance. The Chl-*a*-normalized biological production rates of isoprene ranged from 13.4 to $38.5 \text{ pmol C}_5\text{H}_8 \mu\text{g Chl-}a^{-1} \text{ day}^{-1}$, with an average of $25.1 \pm 8.3 \text{ pmol C}_5\text{H}_8 \mu\text{g Chl-}a^{-1} \text{ day}^{-1}$. The net photochemical production rates of isoprene (P_{photo}) varied between 1.04 and $1.38 \text{ pmol L}^{-1} \text{ day}^{-1}$, with an average of $1.15 \pm 0.15 \text{ pmol L}^{-1} \text{ day}^{-1}$. The column-integrated isoprene production rates in the mixed layer were calculated based on the relationships between isoprene production and environmental parameters. The mean (range) column-integrated isoprene production rates were 207 ± 206 ($111\text{--}611$) $\text{nmol m}^{-2} \text{ day}^{-1}$ and 13.8 ± 1.42 ($12.7\text{--}16.6$) $\text{nmol m}^{-2} \text{ day}^{-1}$ for biological and photochemical production, respectively.

4. Discussion

4.1. Driving Factors of Elevated Isoprene in the KOE

The upwelling in the KOE transported abundant nutrients with a suitable N:P ratio ($\sim 13:1$) from the deep layer to the surface. Additionally, atmospheric

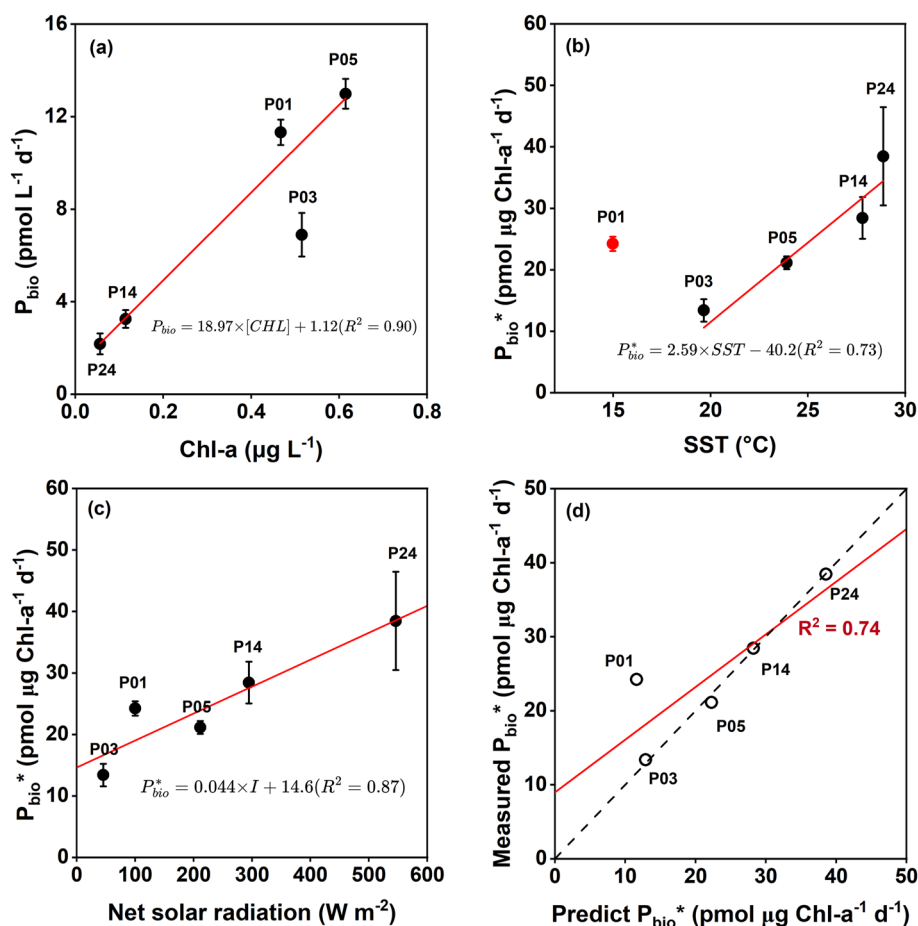


Figure 4. Correlation between biological isoprene production rate and environmental factors. (a) Biological production rate of isoprene (P_{bio}) versus Chl-*a* concentration ([CHL]). (b) Chl-*a* normalized rate of isoprene biological production (P_{bio}^*) versus SST. (c) P_{bio}^* versus light intensity (I). Error bars indicate the standard deviation from triplicate measurements. Red dots with error bars are omitted from the regression calculation. (d) Measured P_{bio}^* versus predict P_{bio}^* from a bivariate linear function ($P_{bio}^* = 0.719 \times T + 0.038 \times I - 2.97$) with SST and I as the independent variables. The dashed line represents the 1:1 line.

particle deposition could also contribute to enriching the euphotic layer with nutrients and supporting relatively high levels of phytoplankton biomass in the KOE (Furutani et al., 2010; Zhang et al., 2019). A significant correlation was found between isoprene and Chl-*a* ($r = 0.47$, $n = 25$, $p = 0.017$). Furthermore, notable correlations between cell density and isoprene concentration were also observed for several specific diatom species, including *C. pelagicus* ($r = 0.420$, $n = 25$, $p = 0.037$), *Chaetoceros debilis* ($r = 0.417$, $n = 25$, $p = 0.038$), *Skeletonema* sp. ($r = 0.404$, $n = 25$, $p = 0.045$), *Guinardia striata* ($r = 0.448$, $n = 25$, $p = 0.025$) and *Cerataulina pelagica* ($r = 0.408$, $n = 25$, $p = 0.043$). Among these species, *Skeletonema* sp. (McKay et al., 1996; Milne et al., 1995; Yassaa et al., 2008), and *Chaetoceros* sp. (Gantt et al., 2009; Milne et al., 1995; Yassaa et al., 2008) have been previously identified as important producers of marine isoprene. Thus, the high phytoplankton biomass (mainly diatoms) in the KOE region fertilized by the supplementary nutrients elevated the biological isoprene production.

Ship-based incubation experiments confirmed the positive effect of nutrient availability on isoprene production. Isoprene concentrations increased approximately 70% and 35% after adding nutrients (equivalent to surface KOE level) and aerosol dust (mimic a strong case of atmospheric deposition) to the oligotrophic seawater. Therefore, well-structured nutrients driven by upwelling in the KOE region are most effective in promoting phytoplankton growth and elevating the isoprene concentration in seawater. Since the KOE region has been reported as one of the areas significantly affected by atmospheric deposition (Furutani et al., 2010; Zhang et al., 2019), dust deposition could potentially serve as an additional driving force to enhance isoprene production.

4.2. Biological Versus Photochemical Isoprene Production Rates

The biological production rates of isoprene were proportional to Chl-*a* concentrations (Figure 4a). Furthermore, the Chl-*a*-normalized biological production rates of isoprene (P_{bio}^* , pmol C₅H₈ μg Chl-*a*⁻¹ day⁻¹) were proportional to the surface seawater temperature (SST) (Figure 4b) and the intensity of solar radiation (Figure 4c). These results indicate that SST and light intensity are important environmental pressures that affect biological isoprene production. This was consistent with the observation of Exton et al. (2013), who reported three distinct SST-dependent relationships between isoprene production and Chl-*a* concentration. Similarly, a clear dependence of isoprene production on light intensity has been illustrated via phytoplankton incubation experiments in a number of laboratory and field studies (Bonsang et al., 2010; Booge et al., 2018; Gantt et al., 2009). The Chl-*a*-normalized biological production rate measured at station P01 became an outlier when plotting against SST. Among the identified phytoplankton species at P01, there were relatively high cell densities of *Fragilariopsis doliolus* (0.8×10^3 cell L⁻¹) and *Asterionella glacialis* (0.4×10^3 cell L⁻¹). Both of them have been reported to be distributed mainly in cold-waters, such as the Antarctic Ocean (Hasle & Syvertsen, 1997) and the North Atlantic Ocean (McMinn, 1995). Their cold-adaptation might support higher isoprene production at lower temperatures, thereby leading to a significant deviation of the biological isoprene production rate (Chl-*a*-normalized) at P01 compared to the other stations when plotted against SST.

During the photochemical incubation experiments of filtered seawater, no significant change in isoprene concentration was observed in the dark groups (Figure S2a in Supporting Information S1). This indicated that any isoprene consumption by the few microbes remaining in the filtered seawater within 6 hr can be considered negligible. Thus, by eliminating the influences of phytoplankton and microorganisms, we can attribute the isoprene increase in the filtered seawater under solar radiation (Figure S2b in Supporting Information S1) to the photochemical reaction of DOM. However, it should be noted that the potential photochemical degradation of isoprene during the light cultivation process, as mentioned in the method section, has not been excluded in this study. Consequently, the final photochemical production of isoprene should be regarded as the net production. The net photochemical production rates of isoprene ranged from 1.04 to 1.38 pmol L⁻¹ day⁻¹, with an average of 1.15 ± 0.15 pmol L⁻¹ day⁻¹. In combination with the biological production rate of isoprene, we concluded that the photochemical production of isoprene accounted for approximately 14% of the total production in this study. More specifically, the proportions of photochemical production of isoprene were approximately 10% and 30% in the KOE and the subtropical NWPO, respectively. This suggests that the contribution of photochemical production is more important in oligotrophic regions characterized by low phytoplankton abundance.

4.3. Underestimation of Isoprene Production in the Marine Environment

We compared the directly determined production rates of isoprene (25.1 ± 8.3 pmol C₅H₈ μg Chl-*a*⁻¹ day⁻¹) with previous reports. Laboratory isoprene production rates determined using individual or multiple phytoplankton species incubations exhibited significant variation, differing by more than two orders of magnitude ($0.72 \sim 32.1$ pmol C₅H₈ μg Chl-*a*⁻¹ day⁻¹) (Bonsang et al., 2010; Exton et al., 2013; Gantt et al., 2009; Meskhidze et al., 2015; Shaw et al., 2003). The mean phytoplankton production rates in the upper 200 m of seawater were estimated to be 4.20 ± 2.76 and 2.40 ± 1.56 pmol C₅H₈ μg Chl-*a*⁻¹ day⁻¹ for diatoms and nanophytoplankton, respectively, using simulations employing a parameterized function of isoprene production rates (Conte et al., 2020). Recently, Simó et al. (2022), operating under the assumption of steady isoprene concentrations over a 24-hr period, determined the isoprene production rates in surface seawater by quantifying loss rates (microbial consumption, ventilation, and vertical mixing), revealing a range from 1.1 to 37.9 pmol C₅H₈ μg Chl-*a*⁻¹ day⁻¹. The results obtained in this study are generally at the high end or higher than the ranges presented in these previous reports.

Furthermore, we computed the isoprene production rates according to the parameterizations and models proposed by Booge et al. (2018), Conte et al. (2020), Ooki et al. (2015), Palmer and Shaw (2005), and Simó et al. (2022), respectively. Those results are denoted using the format “Author’s rate,” like Palmer’s rate. Palmer’s and Conte’s rates were estimated based on the given Chl-*a*-normalized production rate, while the other rates were indirectly obtained by quantifying isoprene loss processes. Detailed calculations are available in Text S1 in Supporting Information S1, and the specific results are shown in Table S2 in Supporting Information S1. As depicted in Figure 5, Palmer’s, Ooki’s, Booge’s, and Simó’s rates were all lower than those determined in the deck incubations, whereas Conte’s rate was higher. This discrepancy primarily arose from the application of higher Chl-*a*-normalized production rates by Conte et al. (2020). Ooki’s method only relies on the sea-to-air

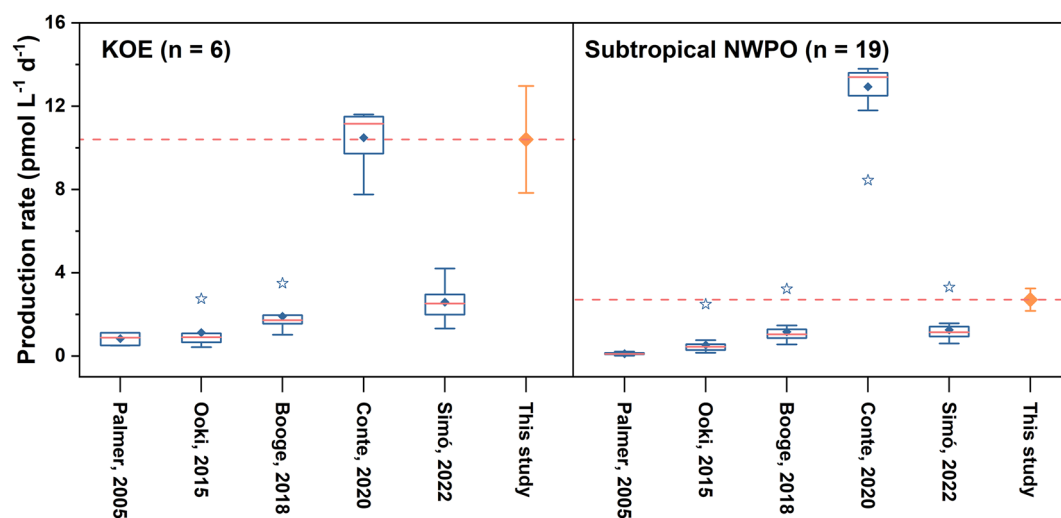


Figure 5. Comparison of isoprene rates calculated using reported methods with the directly determined results in this study. Rates for the Kuroshio Oyashio Extension (KOE) and the subtropical Northwest Pacific Ocean (NWPO) are shown separately, divided by the vertical black line. The lines in the boxes represent the 25th (bottom), 50th (middle), and 75th (top) percentiles, respectively. The whiskers represent the highest and lowest values. The stars represent outliers. The orange diamonds (error bar) represent the mean production rates (SD) determined directly in this study.

flux to estimate the net production rate, whereas Booge's method also considered chemical consumption. Simó's method encompassed all known removal pathways, including ventilation, biological and chemical consumption, and physical vertical mixing, when quantifying the production rate. With the inclusion of more removal pathways of isoprene, estimates from Ooki, Booge, and Simó improved and approached the directly determined rate in this study. Notably, Conte's rate was higher in the subtropical NWPO than in the KOE, which was inconsistent with the other rates. This discrepancy was influenced by the temperature dependent of Conte, as higher SST in the subtropical NWPO elevated the biological isoprene production rate. In summary, there were various contributing factors to the disparities between estimated and measured rates. Therefore, direct measurement of isoprene production rates is highly useful and necessary to improve modeled results.

The comparative results above indicate that the majority of the previously estimated isoprene production rates in seawater were significantly lower than the directly measured values. Additionally, the photochemical degradation

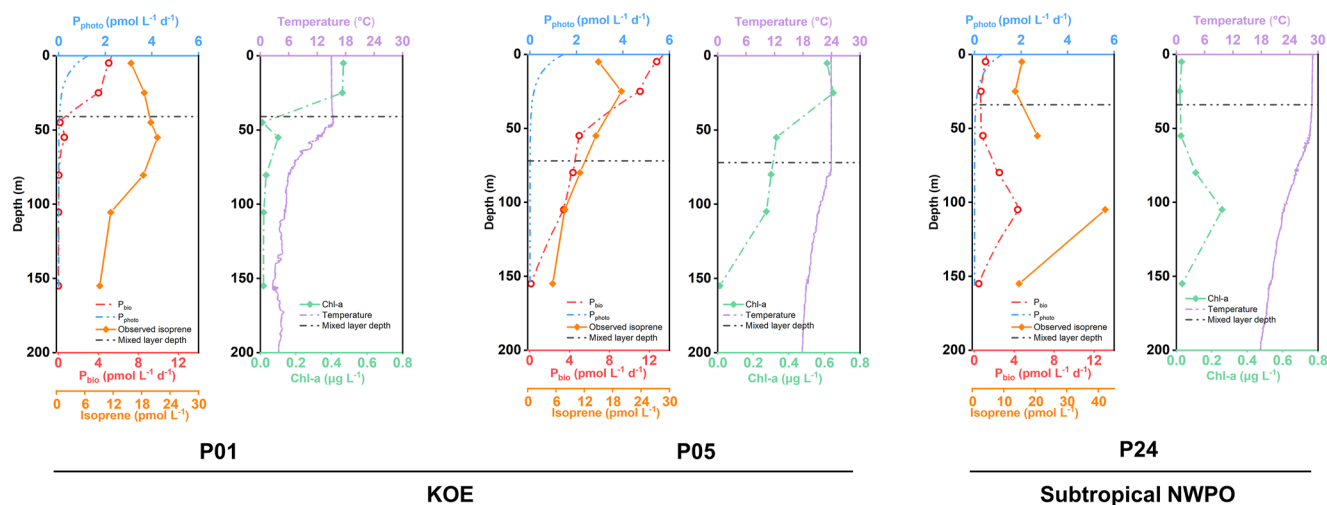


Figure 6. Modeled production rate of isoprene in the mixed layer in the Kuroshio Oyashio Extension (KOE) (P01, and P05) and the subtropical Northwest Pacific Ocean (NWPO) (P24). Blue lines are photochemical production rates, red lines are biological production rates, and orange lines are the observed isoprene concentrations. Green points are the Chl-*a* concentration of seawater at sampling depth. Purple and green lines show the temperature and Chl-*a* used in model rate calculation.

of DOM, serving as a notable abiotic source of isoprene, has always been overlooked. Thus, the isoprene production in marine environments may have been consistently underestimated.

4.4. Assessment of Isoprene Production Within the Mixed Layer

Figure 6 illustrates the vertical variation of modeled isoprene production rate in the seawater column. The modeled production rate closely mirrors the vertical distribution of the observed isoprene concentration, suggesting the feasibility of describing the isoprene production rate using this method. This study identified two distinct vertical production patterns. In the KOE (stations P01 and P05), isoprene production was mainly concentrated within the mixed layer, while it dramatically declined below the mixed layer. Conversely, in the subtropical NWPO (station P24), isoprene production was constrained within the mixed layer, but relatively higher production rates were mainly found below the mixed layer peaking at a depth of around 100 m. The mixed layer in the KOE benefited from a relatively abundant supply of nutrients due to upwelling (introduced in Section 3.1), which supported phytoplankton growth and consequently enhanced the isoprene production. In contrast, the mixed layer in the subtropical NWPO experienced almost full depletion of nutrients. This promoted the phytoplankton to reside in deeper layers to access the necessary nutrients for growth, thereby influencing the vertical characteristic of isoprene production.

4.5. Oceanic Emissions of Isoprene

The sea-to-air fluxes of isoprene ranged from 21.1 to 59.2 nmol m⁻² day⁻¹ in the NWPO, with an average flux of 38.9 ± 13.9 nmol m⁻² day⁻¹. Based on the column-integrated isoprene production calculations, approximately 10%~63% of net isoprene produced in the mixed layer was transferred to the atmosphere, emphasizing the significant contribution of oceanic emission to atmospheric isoprene. A global oceanic isoprene budget simulated by Conte et al. (2020) estimated that 0.27 Tg C of isoprene is annually transferred to the atmosphere, constituting around 60% of the total production within the mixed layer. However, to balance the isoprene budget in the mixed layer, an additional mechanism or sink is required for the remaining portion of isoprene. For constructing the isoprene budget in the mixed layer, a variable biological K_{loss} (ranging between 0.01 and 0.1 day⁻¹) was considered, which was used to reconcile observed in situ isoprene concentrations with the predicted production terms from phytoplankton incubation (Booge et al., 2018). Most recently, it has been reported that isoprene consumption rates in the surface ocean, including microbial consumption and chemical oxidation, are comparable or even greater than ventilation rates (Simó et al., 2022). This suggests that marine isoprene is actively involved in biogeochemical cycles within the ocean interior, potentially serving as a source of energy for microorganisms.

Additionally, larger sea-to-air fluxes of isoprene were found in the KOE (46.0 ± 13.0 nmol m⁻² day⁻¹) compared to the subtropical NWPO (23.6 ± 7.99 nmol m⁻² day⁻¹). Previous field studies in the Northwest Pacific reported similar isoprene fluxes of 41.7 ± 80.4 nmol m⁻² day⁻¹ (Wu et al., 2023) and 43.4 ± 33.8 nmol m⁻² day⁻¹ (Li et al., 2019). From the monthly global maps of calculated isoprene emissions (Booge et al., 2016) in October, a distinct difference between KOE and the subtropical NWPO was found with emissions of ~35 and ~20 nmol m⁻² day⁻¹, respectively. This fitted well with our study. On an annual average, oceanic isoprene emission exhibited spatial variability ranging from 0 to 118 nmol m⁻² day⁻¹, with a global mean flux of 28.7 nmol m⁻² day⁻¹ (Conte et al., 2020). The comparably higher isoprene flux in the KOE can be attributed not only to the elevated production of isoprene in the mixed layer but also to the influence of the extreme physical processes. The KOE, characterized by a plethora of meandering currents and mesoscale eddies, possesses highly intricate hydrodynamics and harbors the majority of the vortex energy in the Pacific Ocean (Wyrki et al., 1976). The vertical motion induced by these eddies enhances the mixing of the upper ocean and promotes the exchange of materials and energy (Volkov et al., 2008). Additionally, eddies can form cold or warm centers, acting as channels between the ocean and atmosphere (Qiu, 2002), thereby fastening the transfer of marine isoprene to the atmosphere. Consequently, due to the combined influence of elevated isoprene production and extreme physical perturbations, the KOE showed relatively high emissions of isoprene, which might significantly alter the atmospheric composition on a local scale.

5. Conclusions

We determined and reported the biological and photochemical production rates of isoprene in the NWPO and examined the links between isoprene and environmental factors. Phytoplankton biomass, temperature, and solar radiation are important factors influencing the biological production of isoprene. Combining direct observations

and incubation experiments, we emphasized the importance of upwelling and atmospheric deposition to supply the nutrients in the KOE surface seawater, which stimulate phytoplankton growth and elevate the isoprene production. Temperature and light intensity are significant environmental pressures on isoprene production. The surface measurements of isoprene concentrations (Chl-*a* normalized) from the whole cruise similarly showed dependency on SST (Figure S3 in Supporting Information S1) as the results from rate experiments from specific locations. Photochemical degradation of DOM in the water column is likely to be an abiotic source of isoprene in the euphotic layer and represents a significant supplement to biogenic marine isoprene production. We modeled the vertical profile of isoprene production, which matched well with the profile of observed isoprene concentrations. The isoprene production rate varied significantly after crossing the mixed layer and displayed different patterns in the KOE and the subtropical NWPO. Numerous regions of the open ocean are oligotrophic in surface, similar to the subtropical NWPO, and isoprene production and distribution in these areas are anticipated to be concentrated below the mixed layer. This suggests that isoprene below the mixed layer is possibly an important portion of the global oceanic isoprene budget. Given the high isoprene production in the mixed layer, the KOE becomes a disproportionately important source of atmospheric isoprene compared to large areas of oligotrophic open ocean, which might have a significant influence on local atmospheric chemistry and climate regulation.

Data Availability Statement

Data presented in this paper are publicly available at Figshare via <https://doi.org/10.6084/m9.figshare.22794617.v1> (Wang, 2023).

References

- Bonsang, B., Gros, V., Peeken, I., Yassaa, N., Bluhm, K., Zoellner, E., et al. (2010). Isoprene emission from phytoplankton monocultures: The relationship with chlorophyll-*a*, cell volume and carbon content. *Environmental Chemistry*, 7(6), 554–563. <https://doi.org/10.1071/en09156>
- Booge, D., Marandino, C. A., Schlundt, C., Palmer, P. I., Schlundt, M., Atlas, E. L., et al. (2016). Can simple models predict large-scale surface ocean isoprene concentrations? *Atmospheric Chemistry and Physics*, 16(18), 11807–11821. <https://doi.org/10.5194/acp-16-11807-2016>
- Booge, D., Schlundt, C., Bracher, A., Endres, S., Zancker, B., & Marandino, C. A. (2018). Marine isoprene production and consumption in the mixed layer of the surface ocean - A field study over two oceanic regions. *Biogeosciences*, 15(2), 649–667. <https://doi.org/10.5194/bg-15-649-2018>
- Carlsaw, K. S., Boucher, O., Spracklen, D. V., Mann, G. W., Rae, J. G. L., Woodward, S., & Kulmala, M. (2010). A review of natural aerosol interactions and feedbacks within the Earth system. *Atmospheric Chemistry and Physics*, 10(4), 1701–1737. <https://doi.org/10.5194/acp-10-1701-2010>
- Ciuraru, R., Fine, L., van Pinxteren, M., D'Anna, B., Herrmann, H., & George, C. (2015). Unravelling new processes at interfaces: Photochemical isoprene production at the sea surface. *Environmental Science & Technology*, 49(22), 13199–13205. <https://doi.org/10.1021/acs.est.5b02388>
- Conte, L., Szopa, S., Aumont, O., Gros, V., & Bopp, L. (2020). Sources and sinks of isoprene in the global open ocean: Simulated patterns and emissions to the atmosphere. *Journal of Geophysical Research: Oceans*, 125(9), 23. <https://doi.org/10.1029/2019jc015946>
- de Boyer Montegut, C., Madec, G., Fischer, A. S., Lazar, A., & Iudicone, D. (2004). Mixed layer depth over the global ocean: An examination of profile data and a profile-based climatology. *Journal of Geophysical Research*, 109(C12), 20. <https://doi.org/10.1029/2004jc002378>
- Exton, D. A., Suggett, D. J., McGenity, T. J., & Steinke, M. (2013). Chlorophyll-normalized isoprene production in laboratory cultures of marine microalgae and implications for global models. *Limnology & Oceanography*, 58(4), 1301–1311. <https://doi.org/10.4319/lo.2013.58.4.1301>
- Frenger, I., Gruber, N., Knutti, R., & Munnich, M. (2013). Imprint of Southern Ocean eddies on winds, clouds and rainfall. *Nature Geoscience*, 6(8), 608–612. <https://doi.org/10.1038/ngeo1863>
- Fry, J. L., Brown, S. S., Middlebrook, A. M., Edwards, P. M., Campuzano-Jost, P., Day, D. A., et al. (2018). Secondary organic aerosol (SOA) yields from NO₃ radical + isoprene based on nighttime aircraft power plant plume transects. *Atmospheric Chemistry and Physics*, 18(16), 11663–11682. <https://doi.org/10.5194/acp-18-11663-2018>
- Furutani, H., Meguro, A., Iguchi, H., & Uematsu, M. (2010). Geographical distribution and sources of phosphorus in atmospheric aerosol over the North Pacific Ocean. *Geophysical Research Letters*, 37(3), 6. <https://doi.org/10.1029/2009gl041367>
- Gantt, B., Meskhidze, N., & Kamykowski, D. (2009). A new physically-based quantification of marine isoprene and primary organic aerosol emissions. *Atmospheric Chemistry and Physics*, 9(14), 4915–4927. <https://doi.org/10.5194/acp-9-4915-2009>
- Guo, C., Yu, J., Ho, T. Y., Wang, L., Song, S., Kong, L., & Liu, H. (2012). Dynamics of phytoplankton community structure in the South China Sea in response to the East Asian aerosol input. *Biogeosciences*, 9(4), 1519–1536. <https://doi.org/10.5194/bg-9-1519-2012>
- Hasle, G. R., & Syvertsen, E. E. (1997). Chapter 2 - Marine diatoms. In C. R. Tomas (Ed.), *Identifying marine phytoplankton* (pp. 5–385). Academic Press.
- Houweling, S., Dentener, F., & Lelieveld, J. (1998). The impact of nonmethane hydrocarbon compounds on tropospheric photochemistry. *Journal of Geophysical Research*, 103(D9), 10673–10696. <https://doi.org/10.1029/97jd03582>
- Hu, Q. H., Xie, Z. Q., Wang, X. M., Kang, H. H., He, Q. F., & Zhang, P. F. (2013). Secondary organic aerosols over oceans via oxidation of isoprene and monoterpenes from Arctic to Antarctic. *Scientific Reports*, 3(1), 7. <https://doi.org/10.1038/srep02280>
- Kloster, S., Feichter, J., Reimer, E. M., Six, K. D., Stier, P., & Wetzal, P. (2006). DMS cycle in the marine ocean-atmosphere system - A global model study. *Biogeosciences*, 3(1), 29–51. <https://doi.org/10.5194/bg-3-29-2006>
- Li, J. L., Zhai, X., Ma, Z., Zhang, H. H., & Yang, G. P. (2019). Spatial distributions and sea-to-air fluxes of non-methane hydrocarbons in the atmosphere and seawater of the Western Pacific Ocean. *Science of the Total Environment*, 672, 491–501. <https://doi.org/10.1016/j.scitotenv.2019.04.019>
- Liakakou, E., Vrekoussis, M., Bonsang, B., Donousis, C., Kanakidou, M., & Mihalopoulos, N. (2007). Isoprene above the Eastern Mediterranean: Seasonal variation and contribution to the oxidation capacity of the atmosphere. *Atmospheric Environment*, 41(5), 1002–1010. <https://doi.org/10.1016/j.atmosenv.2006.09.034>

- Lu, P., McCreary, J. P., & Klinger, B. A. (1998). Meridional circulation cells and the source waters of the Pacific Equatorial Undercurrent. *Journal of Physical Oceanography*, 28(1), 62–84. [https://doi.org/10.1175/1520-0485\(1998\)028<0062:Mccats>2.0.Co;2](https://doi.org/10.1175/1520-0485(1998)028<0062:Mccats>2.0.Co;2)
- Ma, X. H., Jing, Z., Chang, P., Liu, X., Montuoro, R., Small, R. J., et al. (2016). Western boundary currents regulated by interaction between ocean eddies and the atmosphere. *Nature*, 535(7613), 533–537. <https://doi.org/10.1038/nature18640>
- Martino, M., Hamilton, D., Baker, A. R., Jickells, T. D., Bromley, T., Nojiri, Y., et al. (2014). Western Pacific atmospheric nutrient deposition fluxes, their impact on surface ocean productivity. *Global Biogeochemical Cycles*, 28(7), 712–728. <https://doi.org/10.1002/2013gb0004794>
- McKay, W. A., Turner, M. F., Jones, B. M. R., & Halliwell, C. M. (1996). Emissions of hydrocarbons from marine phytoplankton - Some results from controlled laboratory experiments. *Atmospheric Environment*, 30(14), 2583–2593. [https://doi.org/10.1016/1352-2310\(95\)00433-5](https://doi.org/10.1016/1352-2310(95)00433-5)
- McMinn, A. (1995). Comparison of diatom preservation between oxic and anoxic basins in Ellis Fjord, Antarctica. *Diatom Research*, 10(1), 145–151. <https://doi.org/10.1080/0269249X.1995.9705333>
- Meskhidze, N., Sabolis, A., Reed, R., & Kamykowski, D. (2015). Quantifying environmental stress-induced emissions of algal isoprene and monoterpenes using laboratory measurements. *Biogeosciences*, 12(3), 637–651. <https://doi.org/10.5194/bg-12-637-2015>
- Milne, P. J., Riemer, D. D., Zika, R. G., & Brand, L. E. (1995). Measurement of vertical distribution of isoprene in surface seawater, its chemical fate, and its emission from several phytoplankton monocultures. *Marine Chemistry*, 48(3–4), 237–244. [https://doi.org/10.1016/0304-4203\(94\)00059-m](https://doi.org/10.1016/0304-4203(94)00059-m)
- Ooki, A., Nomura, D., Nishino, S., Kikuchi, T., & Yokouchi, Y. (2015). A global-scale map of isoprene and volatile organic iodine in surface seawater of the Arctic, Northwest Pacific, Indian, and Southern Oceans. *Journal of Geophysical Research: Oceans*, 120(6), 4108–4128. <https://doi.org/10.1002/2014jc010519>
- Palmer, P. L., & Shaw, S. L. (2005). Quantifying global marine isoprene fluxes using MODIS chlorophyll observations. *Geophysical Research Letters*, 32(9), 5. <https://doi.org/10.1029/2005gl022592>
- Paulot, F., Henze, D. K., & Wennberg, P. O. (2012). Impact of the isoprene photochemical cascade on tropical ozone. *Atmospheric Chemistry and Physics*, 12(3), 1307–1325. <https://doi.org/10.5194/acp-12-1307-2012>
- Poisson, N., Kanakidou, M., & Crutzen, P. J. (2000). Impact of non-methane hydrocarbons on tropospheric chemistry and the oxidizing power of the global troposphere: 3-dimensional modelling results. *Journal of Atmospheric Chemistry*, 36(2), 157–230. <https://doi.org/10.1023/a:1006300616544>
- Qiu, B. (2002). The Kuroshio Extension system: Its large-scale variability and role in the midlatitude ocean-atmosphere interaction. *Journal of Oceanography*, 58(1), 57–75. <https://doi.org/10.1023/a:1015824717293>
- Ratte, M., Plassdülmer, C., Koppmann, R., Rudolph, J., & Denga, J. (1993). Production mechanism of C2-C4 hydrocarbons in seawater - Field measurements and experiments. *Global Biogeochemical Cycles*, 7(2), 369–378. <https://doi.org/10.1029/93gb00054>
- Seok, M. W., Kim, D., Park, G. H., Lee, K., Kim, T. H., Jung, J., et al. (2021). Atmospheric deposition of inorganic nutrients to the Western North Pacific Ocean. *Science of the Total Environment*, 793, 10. <https://doi.org/10.1016/j.scitotenv.2021.148401>
- Shaw, S. L., Chisholm, S. W., & Prinn, R. G. (2003). Isoprene production by *Prochlorococcus*, a marine cyanobacterium, and other phytoplankton. *Marine Chemistry*, 80(4), 227–245. [https://doi.org/10.1016/s0304-4203\(02\)00101-9](https://doi.org/10.1016/s0304-4203(02)00101-9)
- Siegel, D. A., McGillicuddy, D. J., & Fields, E. A. (1999). Mesoscale eddies, satellite altimetry, and new production in the Sargasso Sea. *Journal of Geophysical Research*, 104(C6), 13359–13379. <https://doi.org/10.1029/1999jc900051>
- Simó, R., Cortes-Greus, P., Rodríguez-Ros, P., & Masdeu-Navarro, M. (2022). Substantial loss of isoprene in the surface ocean due to chemical and biological consumption. *Communications Earth & Environment*, 3(1), 8. <https://doi.org/10.1038/s43247-022-00352-6>
- Stamnes, K. (2015). Radiation transfer in the atmosphere | Ultraviolet radiation. In G. R. North, J. Pyle, & F. Zhang (Eds.), *Encyclopedia of atmospheric sciences* (2nd ed., pp. 37–44). Academic Press.
- Volkov, D. L., Lee, T., & Fu, L. L. (2008). Eddy-induced meridional heat transport in the ocean. *Geophysical Research Letters*, 35(20), 5. <https://doi.org/10.1029/2008gl035490>
- Wang, J. (2023). Isoprene production and its driving factors in the Northwest Pacific Ocean. *Figshare*. <https://doi.org/10.6084/m9.figshare.22794617.v1>
- Wanninkhof, R. (1992). Relationship between wind speed and gas exchange over the ocean. *Journal of Geophysical Research*, 97(C5), 7373–7382. <https://doi.org/10.1029/92jc00188>
- Wennberg, P. O., Bates, K. H., Crounse, J. D., Dodson, L. G., McVay, R. C., Mertens, L. A., et al. (2018). Gas-phase reactions of isoprene and its major oxidation products. *Chemical Reviews*, 118(7), 3337–3390. <https://doi.org/10.1021/acs.chemrev.7b00439>
- Wilke, C. R., & Chang, P. (1955). Correlation of diffusion coefficients in dilute solutions. *AIChE Journal*, 1(2), 264–270. <https://doi.org/10.1002/aic.690010222>
- Wu, Y. C., Gao, X. X., Zhang, H. H., Liu, Y. Z., Wang, J., Xu, F., et al. (2023). Characteristics and emissions of isoprene and other non-methane hydrocarbons in the Northwest Pacific Ocean and responses to atmospheric aerosol deposition. *Science of the Total Environment*, 876, 162808. <https://doi.org/10.1016/j.scitotenv.2023.162808>
- Wyrtki, K., Magaard, L., & Hager, J. (1976). Eddy energy in the oceans. *Journal of Geophysical Research (1896–1977)*, 81(15), 2641–2646. <https://doi.org/10.1029/JC081i015p02641>
- Yassaa, N., Peeken, I., Zollner, E., Bluhm, K., Arnold, S., Spracklen, D., & Williams, J. (2008). Evidence for marine production of monoterpenes. *Environmental Chemistry*, 5(6), 391–401. <https://doi.org/10.1071/en08047>
- Zhang, C., Ito, A., Shi, Z. B., Aita, M. N., Yao, X. H., Chu, Q., et al. (2019). Fertilization of the Northwest Pacific Ocean by East Asia air pollutants. *Global Biogeochemical Cycles*, 33(6), 690–702. <https://doi.org/10.1029/2018gb006146>